



HAL
open science

Prism substructures in the shell of *Pinna nobilis* (Linnaeus, 1758), Mollusca – Evidence for a three-dimensional pulsed-growth model

Jean-Pierre Cuif, Oulfa P Belhadj, Stephan Borensztajn, Marc Gèze, Sergio
Trigos-Santos, Patricia Prado, Yannicke Dauphin

► **To cite this version:**

Jean-Pierre Cuif, Oulfa P Belhadj, Stephan Borensztajn, Marc Gèze, Sergio Trigos-Santos, et al.. Prism substructures in the shell of *Pinna nobilis* (Linnaeus, 1758), Mollusca – Evidence for a three-dimensional pulsed-growth model. *Heliyon*, 2020, 6 (7), pp.e04513. 10.1016/j.heliyon.2020.e04513 . insu-02914596

HAL Id: insu-02914596

<https://insu.hal.science/insu-02914596>

Submitted on 13 Aug 2020

HAL is a multi-disciplinary open access archive for the deposit and dissemination of scientific research documents, whether they are published or not. The documents may come from teaching and research institutions in France or abroad, or from public or private research centers.

L'archive ouverte pluridisciplinaire **HAL**, est destinée au dépôt et à la diffusion de documents scientifiques de niveau recherche, publiés ou non, émanant des établissements d'enseignement et de recherche français ou étrangers, des laboratoires publics ou privés.



Distributed under a Creative Commons Attribution - ShareAlike 4.0 International License



Research article

Prism substructures in the shell of *Pinna nobilis* (Linnaeus, 1758), Mollusca – Evidence for a three-dimensional pulsed-growth modelJean-Pierre Cuif^{a,*}, Oulfa Belhadj^b, Stephan Borensztajn^c, Marc Gèze^d, Sergio Trigos-Santos^e, Patricia Prado^f, Yannicke Dauphin^g^a UMR 7207 CR2P, Muséum National d'Histoire Naturelle, 8 Rue Buffon, 75005 Paris, France^b CRC Ministère de la Culture et de la Communication, Muséum National d'Histoire Naturelle USR 3224, Sorbonne Université, CNRS CP21, Paris, France^c UMR 7154 Institut de Physique du Globe de Paris, 1 Rue Jussieu, 75005 Paris, France^d CeMIM, Muséum National d'Histoire Naturelle de Paris, 43 Rue Cuvier, 75005 Paris, France^e Institut océanographique Paul Ricard, Ile des Embiez, 83140, Six-Fours les Plages, France^f IRTA San Carles de la Ràpita, 43540 Tarragona, Spain^g UMR 7205 ISYEB, Muséum National d'Histoire Naturelle, 45 Rue Buffon, 75005 Paris, France

ARTICLE INFO

Keywords:

Pinna
Mollusca
Prisms
Stepping growth
Biomineralization
Animal physiology
Aquaculture
Materials characterization
Microstructure
Zoology

ABSTRACT

In the shells of the Pelecypods belonging to the Pinnidae family, the calcareous prismatic units of the outer layer are long-standing references for biomineralization studies. To elucidate how the mechanism of prism formation enables both shell elongation and thickness increase, a top-down structural analysis of these classical “simple prisms” has been carried out, taking advantage of shell sampling on actively mineralizing animals. Particular attention was paid to the morphological and structural patterns of the calcareous units sequentially produced at the margins of the growth lamellae. This pre-prismatic part of the shell allows for studying the mineralizing stages not taken into account in prism reconstructions based on samples taken from older areas of the shell. Examination of the microstructural sequence shows that within the actively mineralizing area of the shell, a step-by-step structuring process is continuously running, providing a renewed view of prism formation as it makes obvious the progressive occurrence of their specific patterns. Given the critically endangered status of the species, a better knowledge of the mineralization process associated to shell growth may become handy for future studies aimed at understanding the health status of individuals based on their shell records.

1. Introduction

The mineral units that built the outer layer of the shell in the Pelecypod family Pinnidae (Leach, 1819) are undoubtedly historical references in the research area dedicated to shell microstructures and biological calcifications. In this family, the shells exhibit a rather uncommon organization: due to the much slower growth of the nacreous internal layer, the calcite outer layer forms the main part of the shell. This is illustrated at best by the large well-known noble pen-shell of the Mediterranean species *Pinna nobilis* (Linnaeus, 1758) where the deep-red pigmented outer layer (Figure 1a) largely exceeds the white internal nacreous layer (Figure 1b), making the former easily accessible.

Although apparently massive when viewed on fractures (Figure 1e, f), the Pinnidae prism comprises an acid-resistant organic envelope surrounding its mineralized part (Figure 1g). Occurrence of polarization

microscopy revealed another character that largely contributed to draw attention to the Pinnidae prisms: in transmitted polarized light and between crossed-nicols each prism exhibits a single-crystal behaviour (Figure 1h). These simple and easily accessible characters explain why the Pinnidae prisms were considered as “simple prism” references since the beginning of microstructural studies.

In the first microstructural analyses carried out by Bowerbank (1844) and Carpenter (1844), both took advantage of these favourable features of the Pinnidae: “The structure of the outer layer may be conveniently studied in the shell of *Pinna*, in which it commonly projects beyond the inner, and there often forms laminae sufficiently thin and transparent to exhibit the general nature of its organization without any artificial reduction” (Carpenter, 1856, p. 589). In remarkable series of hand-made drawings produced in the middle of the 19th century, some most

* Corresponding author.

E-mail address: jean-pierre.cuif@orange.fr (J.-P. Cuif).

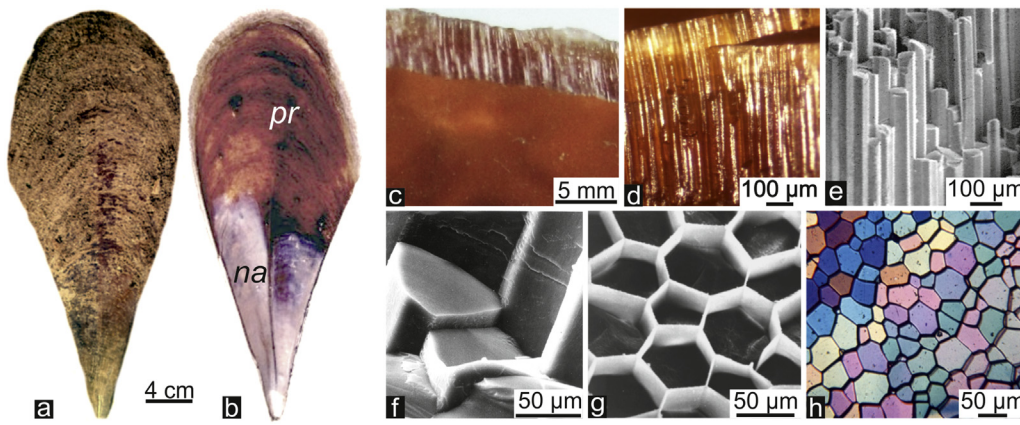


Figure 1. Main microstructural patterns of the outer layer of *Pinna* shell. a, b: External and inner surfaces showing the unusual preponderance of the deep red outer prismatic layer. c–f: Fractured surfaces in the outer layer: (c, d: natural light; e, f: SE SEM). g: Peripheral organic membrane visible after an acidic etching, SE SEM. h: Thin section viewed in transmitted polarized light. Owing to the very high refractive index of calcite, primary colours in the Newton scale indicate a 4–5 μm thickness for this thin section. a–d, f–h: *Pinna nobilis*; e: *Pinna muricata*.

significant (and long forgotten) features of the *Pinna* prisms were already illustrated (Figure 2).

However, beyond their remarkably simple morphology, the regular spatial arrangement and crystalline appearance of the mineral phase, some unusual properties have long suggested that the calcite simple prisms of the Pinnidae may result from a developmental process quite distinct from classical crystallization.

The single-crystal behaviour of the calcite in the *Pinna* prisms under transmitted polarized light is not consistent with the absence of cleavage plans (with fixed angular values between them) that should appear when a *Pinna* prism is fractured if it was a simple calcite crystal. This occurs in the *Pinna* prisms as it does in any other “bio-crystal” (Towe, 1967; Lowenstam and Weiner, 1989). In addition to this abnormal crystallographic feature, *Pinna* prisms have long been recognized as composite materials. Since the earliest observations dealing with shells and other calcareous structures produced by living organisms, the presence of organic materials associated to the mineral material was recognized (e.g. Réaumur, 1709; Hatchett, 1799; Frémy, 1855). Interpretations of this intriguing property have changed through decades of technical improvements.

For instance, after the general acceptance of the cellular theory (Schleiden, 1838; Schwann, 1839), when Bowerbank and Carpenter started the microscopic approach of the shells, they interpreted what they have seen and drawn as cellular components (e.g., Bowerbank, 1844, p.125; Carpenter, 1844, p. 5) (Figure 2c). After recognition that calcification of the shells does not occur inside the cells of the mineralizing organ, but is comparable to a secretion (e.g., Huxley, 1880; Moynier de Villepoix, 1892), the question of an extra cellular control of

crystallization becomes even more intriguing. During the 20th century, through concomitant progresses in observation methods and biochemical characterizations, the stratified structures in the prisms (Bowerbank, 1844, see Figure 2b; Carpenter, 1856, see Figure 2e, f) were explained by repeated deposition of organic layers by the mantle (Grégoire, 1961, 1967, 1972): every layer with a specific biochemical composition (high concentration in acidic amino-acids: Weiner, 1979) acts as a substrate for the consecutive formation of a mineral layer.

In the early 1980's, new data about the distribution of these organic compounds within the mineralized part of the prisms were obtained at infra-micrometric level by scanning electron microscope (SEM) observations of the calcite prisms of *Pinna nobilis*, submitted to symmetrical etching methods inspired by the Mutvei's approach for the ultrastructure of the nacreous units (Mutvei, 1970).

Action of light acidic solutions complemented by fixative mixtures has revealed that the distribution of the intra-prismatic organic component forms a continuous network within the mineral layers, not only between them (Figure 3a, b). Note that the inner surface of the envelope is distinct from the internal organic network. Similar features have been observed in the prisms of a related species: *Atrina rigida* (Nudelman et al., 2007; Addadi et al., 2008). Continuity of these organic components is assessed by the results of the reversed etching based on sodium hypochlorite or enzymes, that dissolve the organic components of the prisms, establishing also the basically granular structure of the mineral components and the regular arrangement of the infra-micrometric mineral units (Figure 3c, d) (Cuif et al., 1980, 1981; Cuif and Raguideau, 1982).

Thirty years later, occurrence of atomic force microscopy (AFM) brought an additional contribution to the knowledge of the infra-

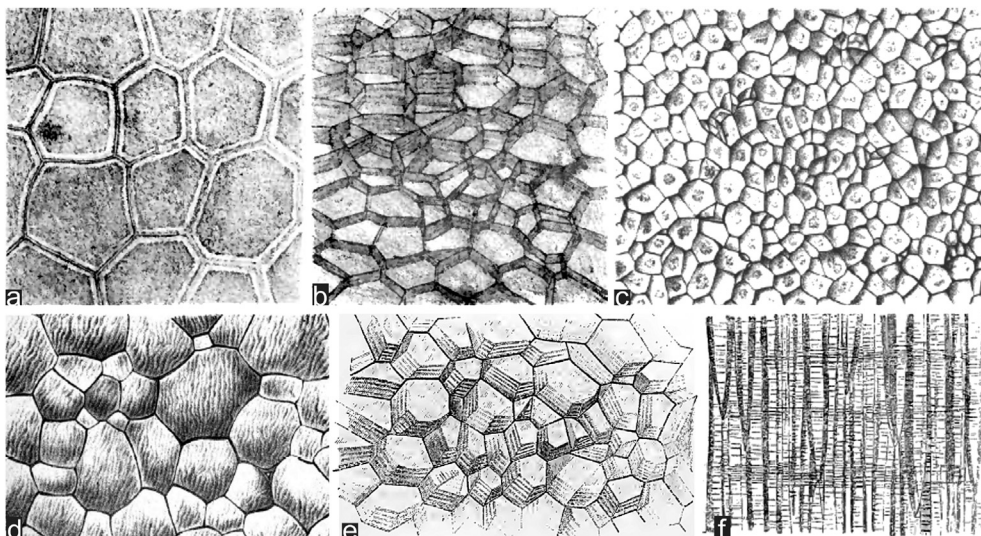


Figure 2. Prisms of Pinnidae. a: Transverse section showing the polygonal shape of prisms and the thick envelope (from Bowerbank, 1844). b: Oblique fracture showing the inter-prismatic organic membranes (from Bowerbank, 1844). c: Aspect of unetched surface showing central differentiation (compare to Figure 5e) (from Carpenter, 1844). d: Inner surface of the shell showing parallel ridges and grooves (compare to Figure 6) (from Carpenter, 1844). e: Oblique section showing the polygonal shape of the prisms and internal growth lines (from Carpenter, 1856). f: Radial section showing the prism envelopes and transverse prism growth lines (from Carpenter, 1856).

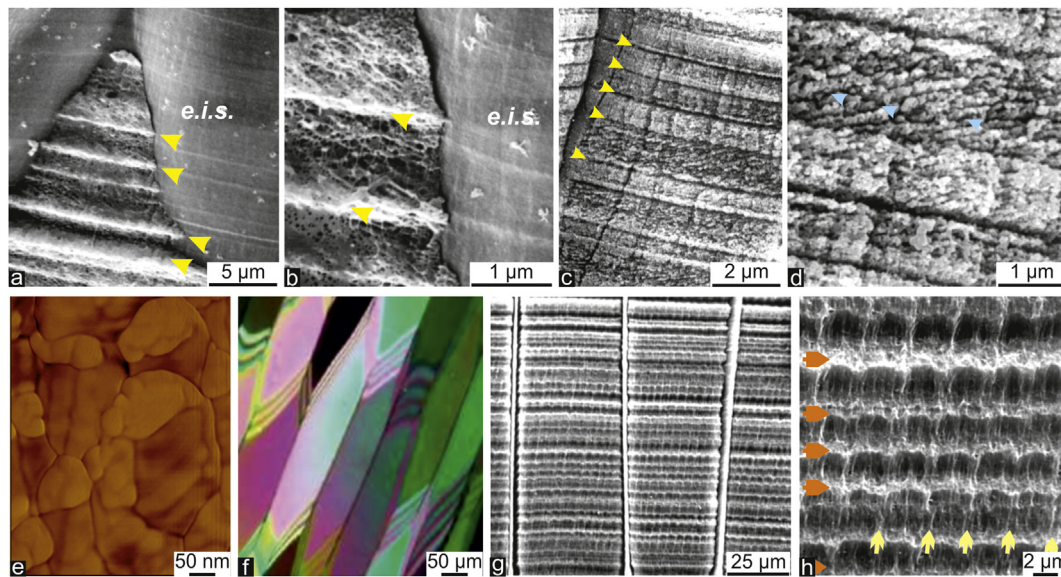


Figure 3. Composite organization of the *Pinna* prisms at the infra-micrometre level. a, b: *Pinna muricata*: the inner surface of the organic envelope (*e.i.s.*) shows the remains of the major growth steps (yellow arrows), and an irregular organic network between them. Fixation: glutaraldehyde 6%, Na cacodylate 0.4M, NaCl 7% for 1 h at 8 °C, rinsed using Na cacodylate 0.4M, NaCl 7%, then etched in RDO for 5 s, rinsed with Milli-Q water. SE SEM images. c, d: The main concentration of organic compounds between the growth layers and the specific arrangement of the infra-micrometric calcareous grains within the growth layers visible after a chemical or enzymatic etching. SE SEM images. e: Granular structure of the prism. Unetched sample. AFM phase contrast image. f: Crystalline aspect of the prisms in longitudinal (slightly oblique) thin section (transmitted polarized light). g, h: Longitudinal structures within prisms; the crossed directions for assessing a three-dimensional control of the shell growth. *Pinna nobilis*, fixation, etching: glutaraldehyde 12% (100 ml) acetic acid 1% (1 ml) Alcian blue 0.05% (1 ml) 6 min, room temperature. SE SEM images.

micrometric granular structure of the mineral phase within the prisms. While the dissolution process inherent to any etching method prevents obtaining precise information about the relationship between the organic component and the surface of the sub-micrometre-sized grain, this new method allows demonstration of the composite structure of the prism material without any etching. Phase contrast imaging (Figure 3e) shows individual grains with an irregular round-shaped morphology without any cleavage plans. Grains 50–100 nm in diameter are coated by a thin cortex that strongly interacts with the AFM tip, at the difference of the mineral particles (Dauphin et al., 2018).

Contrasting with the morphological simplicity of the prisms of *Pinna nobilis* and their single crystal behaviour (Figure 3f), the etching experiments have also revealed a series of longitudinal structures slightly oblique with respect to geometry of the prisms (Figure 3g, h). These structures suggest that beyond the simple repeated deposition of the micrometre-thick growth layer that built the outer shell layer, an additional mechanism may exist.

In this study, a top-down approach to the thin mineralized structures that repeatedly appear at the growing edge of the *Pinna nobilis* shell is carried out. Taking advantage of samples collected on actively mineralizing specimens, an attempt is made for reconstructing the sequence of microstructural events by which these distinct growth lamellae are formed and incorporated into a compact three-dimensional prismatic layer. New evidence for a longitudinal micrometric stepping growth process of the shell justifies ancient and neglected observations. Additionally, fine scale data about the crystalline structure of the prisms explain how simultaneous elongation and thickness increase of the shell outer layer can be obtained.

2. Material and methods

2.1. Material

Living specimens of *Pinna nobilis* were collected in two distinct places of the western Mediterranean Sea: on the shore of Les Embiez Island (Paul Ricard marine institute for environmental survey, Six-Fours les

Plages, France) and at the Alfacos bay of the Ebre delta (Catalunya, Spain). Samples of *Pinna muricata* Linnaeus, 1758 come from the SW coast of Madagascar (Tulear). This species is smaller than *P. nobilis*, and the shell is mostly white.

The samples were collected in the actively mineralizing areas of the shells, each of them comprising two to four of the distal growth lamellae with about 1–3 cm in width. Samples were placed in ethanol/sea water solutions with three concentrations: 30/70 for 6 h, 60/40 for 12 h, then 6/7 days for the last 90/10 mixture.

2.2. Optical microscopy

Optical microscopy includes examination in transmission mode (both polarized and non-polarized light) of sections perpendicular or parallel to the surface of the prisms.

Polarized light microscopy in the reflected (episcopic) mode has been shown of special interest, making crystallinity of prisms visible in polished sections. An Axio Imager D2m (Zeiss) was used with the Archimed software (Microvision).

2.3. Confocal microscopy

Confocal Z-series stacks of the polished surfaces of the prismatic layer were acquired on a Zeiss LSM 880 point scanning confocal microscope using the Airyscan detector, a 20x Plan-Apochromat, and the 488 nm and 561 nm laser lines. The Zeiss Zen 2.3 software was used to control the microscope, adjust spectral detection and for processing of the Airyscan raw images. Images were also processed using Fiji.

2.4. Scanning electron microscopy (SEM)

Scanning electron microscopy observations were made in secondary (SE) and back-scattered (BSE) observation modes, using different instruments: Philips XL30 SEM, a FEG-FIB-SEM AURIGA 40 Zeiss, a FEI FESEM Quanta F600, and a table top FEI PHENOM Pro X. Polished sections were prepared by using diamond grade suspensions, lightly etched

using a weak acidic solution. BSE consists of high-energy electrons reflected or back-scattered out of the specimen. Since atoms with a high atomic number Z have stronger scattering power than light ones, the mineral rich areas appear brighter than zones rich in organic matters. So, such images contain compositional information.

2.5. Atomic force microscopy

Samples were studied using a Nanoscope IIIa multi-mode scanning probe microscope. No coating is required: AFM utilizes an oscillating tip in both height and phase-contrast modes. Resolution of tapping mode is in the few nanometre range. In the phase contrast mode, the image contrast is due to physical interactions between oscillating tip and the studied substrate. Compositional heterogeneity results in difference in interaction, causing phase-lag transcribed into white to black values (an appropriate capability for establishing small scale distribution of organic components within biominerals): a soft material is usually “darker” than a hard material (Haugstad, 2012; Mittal and Matsko, 2012).

3. Results

At the outer surface of the *Pinna* shells the series of parallel major growth steps marked by the upward oriented and curved scales (Figure 4a, b: white arrows) was built by the repeated onward/backward movements of the mantle by which the animal extends the lateral dimensions of its shell. A longitudinal section of the distal edge perpendicular to shell plane (Figure 4c) shows that the upward oriented scales are the final stages of the shell growth units. Their initial stages begin inside the shell, because at the end of its backward movement the periostracum is glued onto the internal surface of the valve, a few millimetres inside the shell. When environmental conditions allowed for opening of the shell, the specialized cells in the deeper part of the outer mantle groove start the secretion of the new periostracal membrane, providing space for a forward movement of the mantle.

The early stage of the process is illustrated through close frontal view of the shell (Figure 4d, e). Two almost circular scales are visible (Figure 4d: green arrows). They show at their basis a thin membrane that is the starting new growth lamella (Figure 4d: red arrows), freely onward growing between the two neighbours upward inflexions marking the end of the previous growth lamella. From inside the shell (Figure 4e) the newly growing lamella appears as an almost flat continuous surface

(Figure 4e, g). From outside the shell, this newly growing structure becomes visible only when its size exceeds the distal growth edge of the previous growth unit. These pictures were obtained from remarkably well-preserved sectors of the shells of dead animals. On an actively mineralizing animal, the illustrated structures are not visible: they are included within the mineralizing compartment displayed in Figure 4f. On Figure 4g, the series of yellow arrows marks the onward moving line by which the continuously growing periostracum produced in the outer mantle groove is submitted to a full backward inflexion, because attachment of the periostracum to the previous growth unit (green arrows) creates a fixed point.

Between these yellow and green arrow lines, the successive steps of the mineralization sequence producing a growth lamella can be investigated through a reverse examination, from its earliest stages up to formation of the first prisms. Therefore, availability of the mineralized structures produced within this closed compartment enables examination of structures usually not included in microstructural descriptions based on collection specimens of the *Pinna* shell.

3.1. A dual calcification occurs in the early developmental stage of the growth lamella: calcareous disks brought by the periostracum are cemented through an additional calcification

In the developmental history of a *Pinna* shell, each of the distinct scales was a temporary growing edge whose upward inflexion indicates the maximal extension of the animal mantle (Figure 5a, b). Note that each of this onward developmental progression was also a stepping process (Figure 5b, arrows). Examination of the distal area of an upward scale reveals the presence of distinct circular units (Figure 5c) firstly accumulated in a somewhat disordered arrangement, but immediately cemented by additional deposition of calcareous materials (Figure 5d, e). This stabilization process can be more clearly evidenced through transmitted polarized light (Figure 5f–h) showing that transformation of the accumulated disks into a solid structure occurs by adjunction of calcareous material deposited by a pulsed process. Sometimes (e.g., Figure 5g, h), the pulse calcification process is assessed by a visible synchronism in the mineral accretion between neighbour units. Progressively, this mineral deposition occupies the remaining free spaces between the initially round-shaped centered disks, resulting in a compact but roughly irregular microstructures.

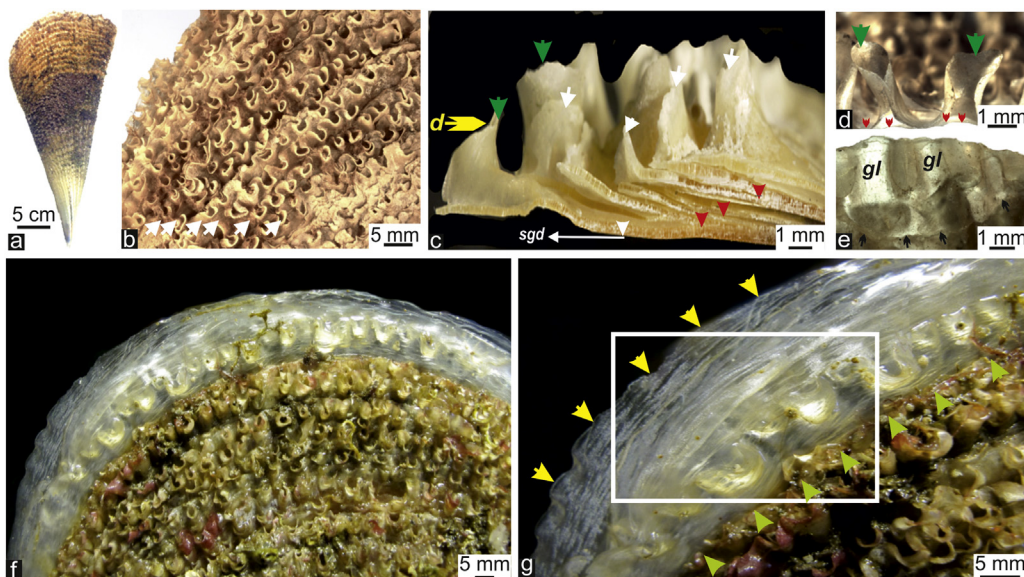


Figure 4. Pulsed growth mode at the macro-scale and aspects of the actively mineralizing area. a, b: Regularity of the successive upward inflexions of the growth lamellae at their final growth stage (a: juvenile specimen). c: Section at the growing margin of the shell showing the series of growth lamellae (white arrows) starting from the inside of the shell at various distances depending on intensity of the mantle retractions (red arrows). d: Frontal view of the growth margin. Two upward inflexions of the previous growth layer are visible (green arrows); note the flat early beginning of the next growth lamella (red arrows). e: Internal view of the newly growing lamella. f: Overall view of an actively mineralizing *Pinna nobilis*. g: Enlarged view between the line of the periostracum backward inflexion (yellow arrows) and the attached periostracum (green arrows). Note the stepping growth mode of the periostracum. gl: growth lamella, sgd: shell growth direction.

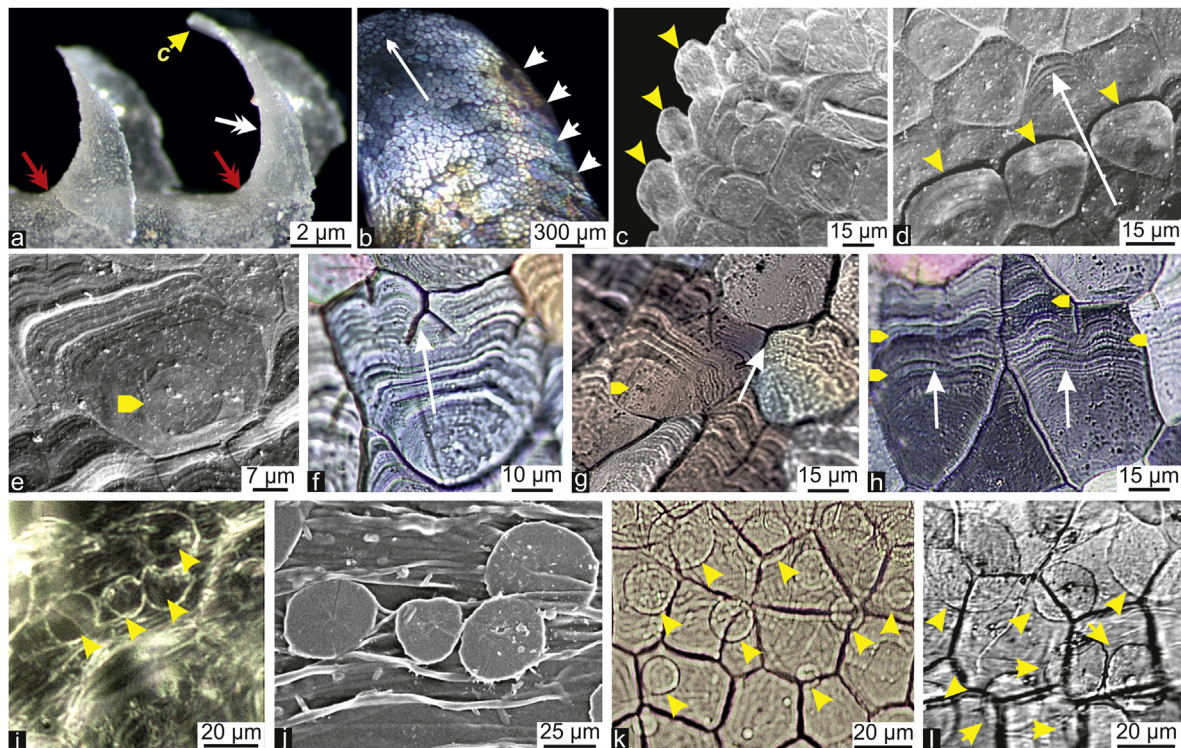


Figure 5. Dual origin of the growth lamellae observed at their terminal stages. a: Two consecutive upward-oriented inflexions of the growth lamellae (lateral view). Each growth unit comprises two distinct phases because the upward inflexion is preceded by a rectilinear phase that ensures shell extension (between the red arrows). (b): The pulsed mode at the infra-millimetre scale is well exposed by transmitted light. (c): SEM view of the periostracal disks that were initiated and grown inside the shell in the outer mantle groove. (d–h): Completion of the intervals between the periostracal disks by deposition of epitaxial calcium carbonate. d,e: SEM view. (f–h): Transmitted polarized light reveals the irregular morphology of the resulting units and consistency of their individually specific polarization color. Note their sometimes synchronous deposition between two adjacent units. (i–l): Various views of the periostracal disks (yellow arrows) still attached to the periostracum outside the shell: (i) numerical microscope; (j) scanning electron microscope; (k) optical microscope natural light; (l) confocal microscope.

In every composite unit formed by an initial disk and the cementing material, both disk and additional material exhibit identical polarization colours. This shows that in each case the newly secreted calcareous material has adopted the crystallographic orientation of the discoid unit in contact with which it was deposited. That crystallographic orientation of the cementing material was driven by contact with the preexisting disks provides evidence that the calcium carbonate responsible for disk cementation was secreted as an amorphous material (see also below 4.3.2: Prism crystallization).

Surprisingly, circular disks can be sometimes observed at the outer surface of the growth lamella, superposed to the polygonal structure (Figure 5i–l). This apparently abnormal location is directly linked to the repeated movement of the mantle. At the end of a growth period, when the mantle backward movement occurs, the periostracum (that ensures anatomical continuity between the mantle and the shell) is disrupted. One part is retracted with the mantle within the shell whereas the other part remains attached to the shell. With respect to shell formation these circular disks are lost because they will not be incorporated into the next growth layer. Therefore, they will be visible as isolated elements superposed to polygonal components of the newly growing lamella (Figure 5c–f).

But in the normal course of shell growth (i.e., without periostracum disruption), these circular disks grown during the transit of the periostracum arrive to the shell margin and contribute to formation of the growing lamella.

3.2. Occurrence of the Voronoi pattern: initiation of the prismatic microstructure

At the lower part of the growth-scales (Figure 5a, white double arrow) the disordered arrangement of irregularly calcified units is followed by a

strikingly different pattern: the microstructural units are now morphologically well defined, forming an assemblage in which every polygonal unit behaves as a single crystal when observed in transmitted polarized light (Figure 6a, b).

Observed in natural light, this new mineralized area offers a remarkable example of the Voronoi tessellation. This polygonal figure is obtained by joining a series of irregularly distributed points (Delaunay triangulation) and drawing a perpendicular line in the middle of the resulting segments. A classical physical example of such a phenomenon is given by waves from neighbour emitting centres. Occurrence of the new microstructural pattern now visible in the *Pinna* growth scales belongs to a comparable process, and drives attention to the distinctly visible nodules located in position of the “emitting sources” (Figure 6c, d) with respect to formation of the polygonal organic network.

SEM images show that the comparison can be continued when looking at the mineralized structures: a comparable regular arrangement can be found between the centres and the outer boundaries of the underlying mineralized units (Figure 6e). These earliest polygonal calcareous platelets are also remarkable by the series of lines radiating from their centres (Figure 6f). When the central area of the polygonal units has been removed by natural decay of the overlying tissues or through equivalent oxidative preparative process, the visible central depressions make obvious the place of the initial calcification for every calcareous polygon. The surrounding concentric lines assess for a calcification process concentrically spreading from every polygon centre (Figure 6g). In addition to these pictures of the outer surface of the growth scale, the inner side reveals that polygonal envelopes slightly predate the deposition of the first mineral layer (Figure 6h), with radiating structures also visible within the more advanced mineral deposition (Figure 6i, j).

Figure 6k exhibits the internal growth surface and the lateral sides of a very young prism (still wider than long). The superposed mineral layers

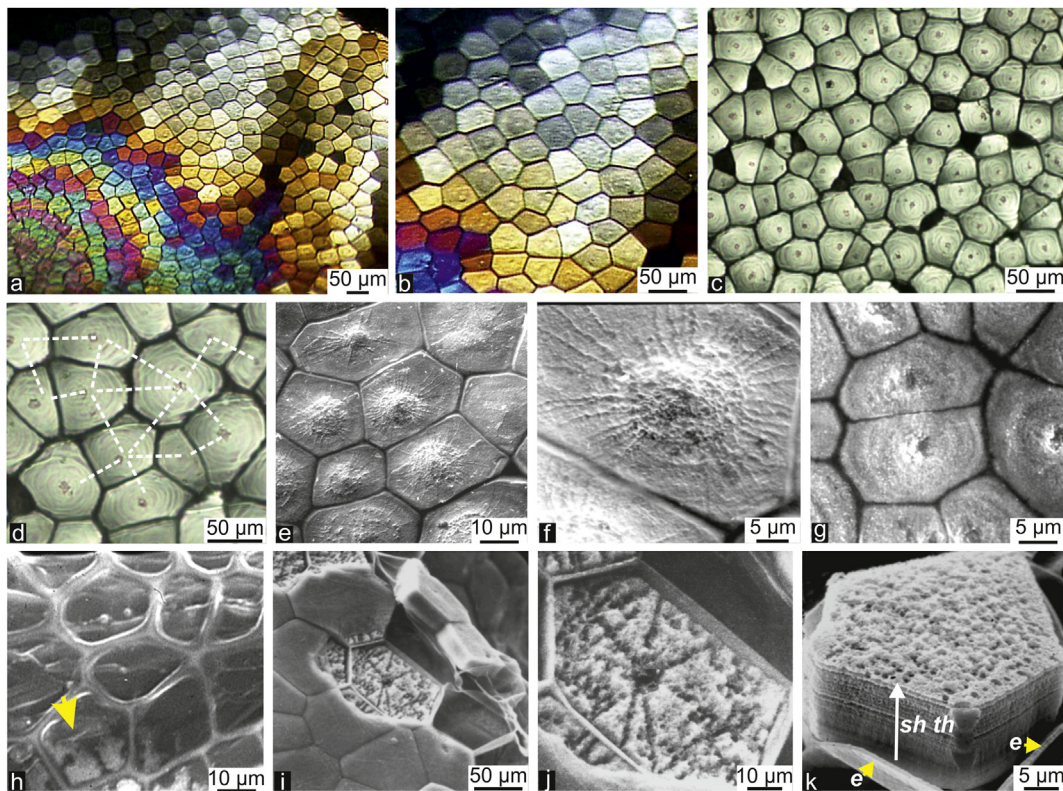


Figure 6. Occurrence of a regular polygonal framework and early prism mineralization. a, b: Optical view (transmitted polarized light) of the second microstructural stage. c, d: Typical Voronoi tessellation between the polygon centres and segments of the adjacent polygons. e, f: First mineralization stages organized from the polygon centres (cleaned outer view of the shell below the periostracum; compare with Carpenter's Figure 2c). g: Traces of the calcification centres and concentric deposition of the calcareous material. h–k: Corresponding growth stage viewed from the inner side of the shell: polygonal organic framework (h), polygon centers and radiating structures (i, j); unetched growth surfaces of young prisms showing the first completed mineralized growth layers (k). e: prism envelope; *sh th*: shell thickening = prism elongation.

are now completed. Lateral sides of the mineral units are freed from the organic envelope. The previous development stages, essential for acquisition of the morphological and crystallographic properties, are no longer visible as they were in the younger stages (Figure 6h–j): clearly the earliest prism structuring phase is over.

In this present status of shell formation, the morphological patterns of a “simple prism” are now gathered (Figure 6k): polygonal envelope associated to a linear layered growth mode of the mineralized material. At this point, attention must be drawn to the century and half old hand-made drawing shown in Carpenter (1856) (Figure 2c), a picture that found striking confirmation in the converging data gathered on Figure 6. However, the structural evolution of the *Pinna* prisms is not completed yet, as shown by the internal surface in the older areas of the shell.

3.3. Evidence for longitudinal substructures in the *Pinna* prisms

More internal areas of the shell show that an additional mechanism becomes active in formation of the prisms: at the difference of Figure 6k, their internal surfaces exhibit a system of parallel ridges and grooves (Figure 7a–c) that shows two remarkable properties:

- (1) In spite of weak irregularities at the individual level, the ridge and groove series are globally parallel to the shell margin (transverse to growth direction of the shell, Figure 7c, d: white arrows).
- (2) More surprisingly, the ridge and groove systems seem synchronically produced across adjacent prisms, despite being interrupted by the prism envelopes (yellow bars on Figure 7e, f).

Note must be made that with respect to the progressive development of shell microstructure, this stepping process occurs after the formation of the initial prisms based on the Voronoi tessellation, organized around well defined centres (Figure 6). In this early stage, growth of the prisms was only perpendicular to the shell surface, whereas the additional mechanism initiates a stepping growth mode that results in lateral extension of the shell. However, epipolarization microscopy (Figure 7g) reveals that the crystallographic individuality of the prisms is preserved. It is also worth to note that the mineralizing surface of the prisms is covered by the Marsh's membrane. This continuous translucent organic film is so closely attached to the shell surface that the ridges and grooves remain visible, although attenuated (Figure 7h) (Cuif and Dauphin, 2018). Existence of corresponding substructures in this membrane is emphasized by epipolarization (Figure 7i). Light etchings provide complementary pictures of the prism inner organization. Distinct sensitivities of organic component to the etching solution provide evidence of an underlying cyclic process, resulting in the alternating ridges and grooves pattern (Figure 7j), although a common microgranular microstructure is visible on both features (Figure 7k). Additionally, an acidic and fixative solution makes obvious that the organic structures are associated with mineral deposition: the spatial arrangement of this intraprismatic organic component reveals a rhythmic deposition process comparable to the cyclic pattern visible in the mineral phase (Figure 7l, m).

This series of data provides the first evidence that a coordinated growth mode exists between the prisms of a given shell valve, a pattern clearly linked to the longitudinal extension of the shell. Again, we can find in the Carpenter's work (see Figure 2d) a picture closely similar to the microstructural data collected here (Figure 7) and below (Figure 8) by using various methods.

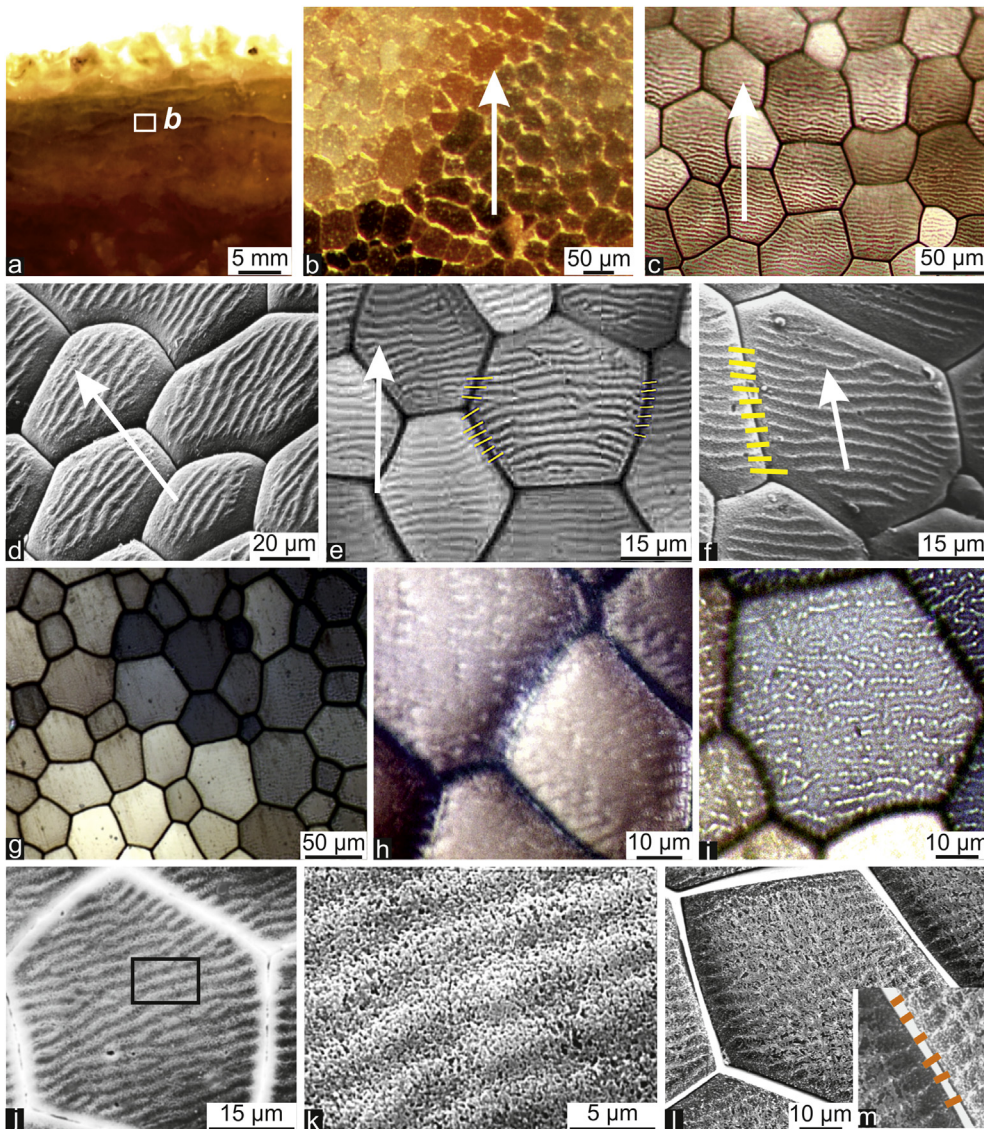


Figure 7. Inner surfaces of the prisms in an actively mineralizing area of the *Pinna nobilis* shell. a–c: Occurrence of ridge and groove system at the growth surface of the prisms, globally transverse to the growth direction of the shell; optical view. d–f: SE SEM view of the ridge and groove system globally parallel to the shell growth margin; d: Cleaned using commercial Na hypochlorite for 17 h at room temperature. g: Growth surface: prisms are individualized through epipolarization microscopy. h: Closer view of surfaces covered by the Marsh's membrane with underlying ridges and grooves. i: Epipolarization view of a prism surface covered by the Marsh's membrane: punctuated growth lines of the Marsh's membrane are well visible. j, k: Light etching showing the micro granular structure of both ridges and grooves of the mineral phase. l, m: Polished, fixed and etched transverse section showing the organic substrate structures correlated to the ridge-groove mode of shell elongation (l) and correspondence of the organic ridges between both sides of the polygonal organic envelope. Fixation, etching: glutaraldehyde 12% (100 ml) acetic acid 1% (1 ml) Alcian blue 0.05% (1 ml) 6 min, room temperature.

3.4. Correspondence between internal and superficial features of the prisms

By dissolving the polygonal organic framework that maintains the mineral units together (using Na hypochlorite or H_2O_2 : Figure 8a), examination of the isolated prisms becomes possible. Complementary information regarding their specific growth mode is brought in addition to the Figure 7 dedicated to their internal surfaces.

On Figure 8b, c, besides the expected series of dense and parallel growth layers that increase the prism length (Figure 8c: *th inc* = shell thickness increase) we also observe on the other side of the same prism, the traces of the concomitant stepping process that has been recorded by the prism envelope (here only partly dissolved). The yellow arrows in Figure 8c (*sgd*: shell growth direction) draw attention to the series of lateral crests oblique to the overall longitudinal axis of the prism. Figure 8d shows the corresponding traces visible on a transverse section. Laser confocal microscopy carried out on growth lamellae (Figure 8e–g) reveals also that both mineralized materials and organic envelopes are involved in this lateral stepping mechanism of the prisms.

Evidence that the lateral stepping growth of the prisms creates a link between each prism and growth direction of the shell is illustrated in Figure 8h–j. When a prism side-face is oriented in conformity with the shell margin line (*i.e.*, perpendicular to growth direction as in Figure 8i: *sgd* and *growth margin*), only the prism growth-layer traces are visible as

parallel lines illustrated in Figure 8h, i (*growth margin*) (see also Figure 9b side-face 3). But when the side-faces of the prism are oblique to the shell growth direction, the traces of the lateral growth steps of the prism become visible as in the prisms pictured in Figure 8h, j. The stronger the obliquity the higher the number of visible lateral growth layers: this is clearly illustrated by irregular prisms in Figure 8e.

This observation leads to an important conclusion: the oblique sub-structures viewed from both the external surfaces (Figure 7c–i) and internal sections (Figure 7j–m) indicate that the early stage in formation of the prisms (Figure 6) is a preparative phase predating the installation of a more complex mineralization process. This new growth mode deserves to be considered as the mature status of the prism because this complex three-dimensional stepping process persists up to the uppermost layers.

4. Discussion

Data provided by the mineralizing area bring substantial changes to the model of *Pinna* prisms commonly viewed as a single pile of mineral polygons, surrounded by an organic envelope and externally covered by a protective organic periostracum. As confirmation of about one hundred and sixty year Carpenter's old schemes (Figure 2) and SEM data (Figure 3), previous results appear now as evidences for the existence of a double stepping growth process in the outer layer of the *Pinna* shell:

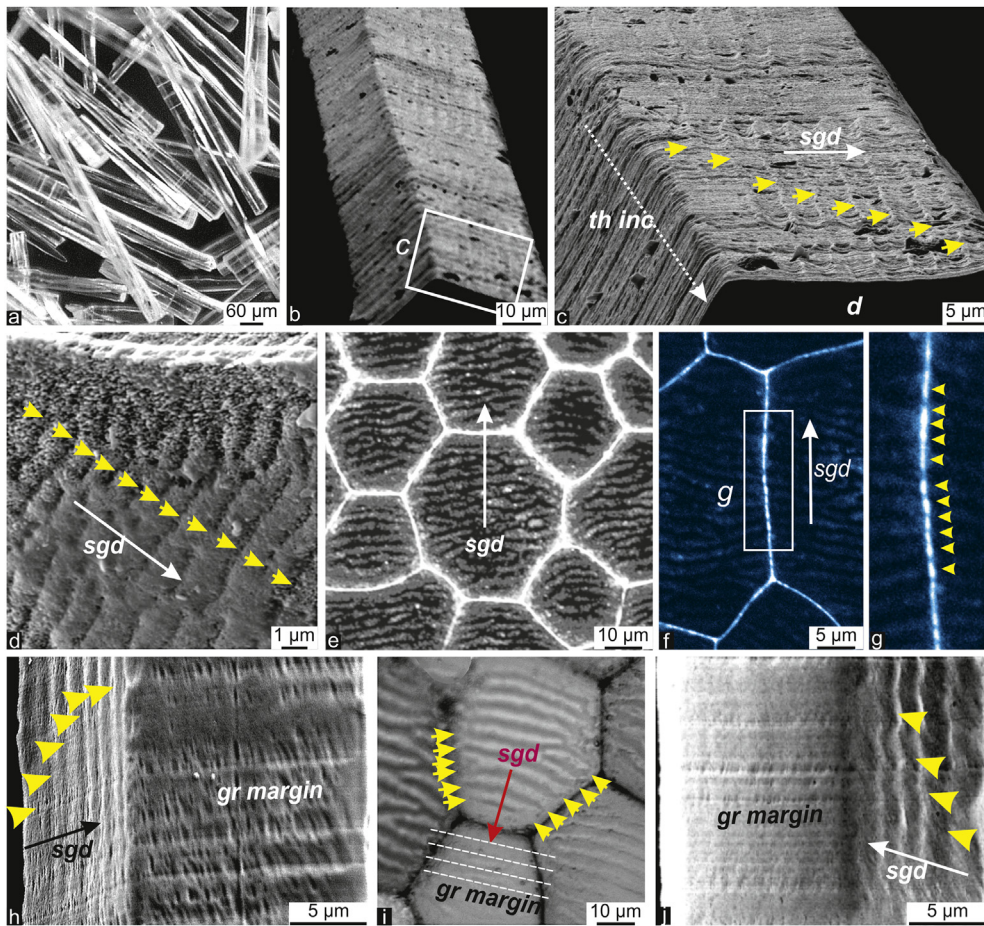


Figure 8. Oriented growth and sub-structures in the prisms according to shell elongation. a: Prisms dissociated by action of Na hypochlorite. b, c: Remains of the polygonal organic framework at the periphery of the mineralized units; traces of the lateral stepping growth stages (arrows) whose orientation is slightly oblique to prism morphology (compare to Figure 2k, 2l) (sgd; shell growth direction). d: Transverse section of the prism: the parallel traces of the lateral growth steps are visible (yellow arrows). e: Evidence of transversal growth steps by laser confocal microscopy carried out on distal growth lamellae. Transverse orientation of internal substructures with respect to shell growth direction (sgd) is maintained between adjacent prisms (to be compared with Figure 2c). f, g: Lateral stepping growth mode of the envelopes is visible (Laser confocal microscopy, excitation wavelength 488 nm). h–j: Lateral growth traces on prism side-faces vary according to their orientation with respect to direction of shell elongation (sgd: stepping mode of the shell growth margin (gr margin)).

- the basic layered biomineralization mechanism ensuring elongation of the prism (Figure 3h, tan arrows)
- a longitudinal stepping growth in the prisms, linked to shell extension (Figure 3h, yellow arrows).

Comments of the three major ontogenic steps that contribute to formation of the *Pinna* prisms draw attention to their complexity, rising question about their role as microstructural reference.

4.1. Periostracal disks: the mineralized components of a “flexible shell” predating the growth lamellae. Comparison with equivalent earliest growth stages in *Pinctada margaritifera* shell

Examination of the *Pinna* growing edge (Figure 5) has illustrated the process by which the distinct round-shaped units at the shell growth line are transformed into a solidified structure by adjunction of specific calcareous material. This process occurs at the periphery of the disks and within the free places between them (Figure 5m–p).

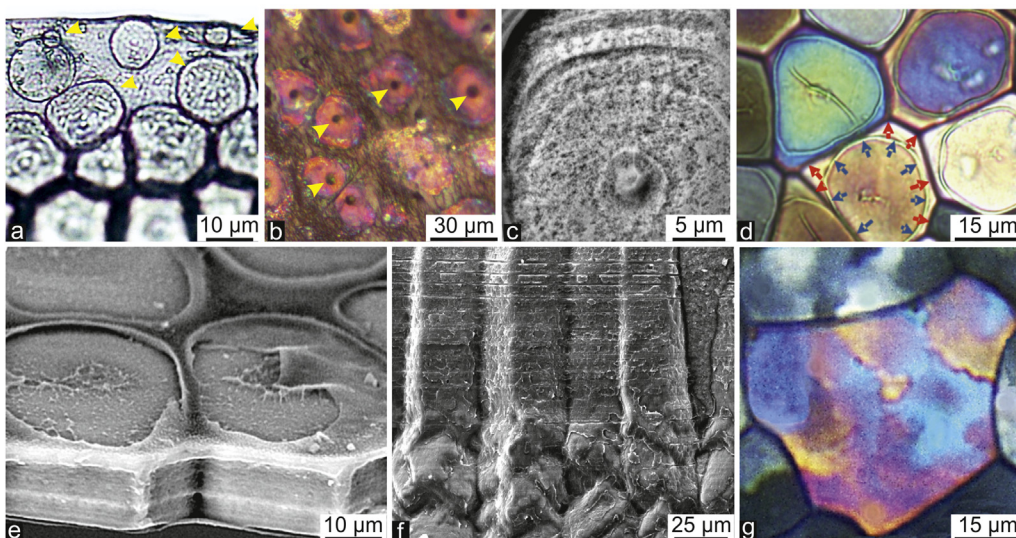


Figure 9. Summary of developmental sequence at the shell growth edge of *Pinctada margaritifera* (from Minerals 2019). a–c: Periostracal disks in distal shell margin: note the concentric growth of the periostracal disks. d–e: Incorporation of the periostracal disks into a rigid shell: cementation of the disks by lateral deposition of Ca-carbonate. f–g: Synchronic changes in prism microstructure assessing evolution of the biomineralization process producing distinct morphology and polycrystalline microstructure for every prism.

With respect to size, shape and position, these circular units are similar to the structures previously described on the periostracum of the *Pinctada margaritifera* shell, the Polynesian pearl oyster (Cuif and Dauphin, 2018). This species also produces an outer shell layer built by calcitic prisms although, compared with the *Pinna* shells, the respective importance of the outer and inner shell layers are in reverse proportions. Worth noting that this structural difference between the two species begins immediately at the “post-disk” step of shell formation, i.e., the species-specific method by which these disks are used as components of the solid shell.

In *Pinctada* the free round shaped units growing by accretion of concentric mineral deposition (Figure 9a–c) are brought to the shell growing edge by the “conveyor-belt” function of the periostracum (Cuif et al., 2018), in a similar mode to what occurs in *Pinna*. Nevertheless, the passage from the “flexible” to “rigid” shell status already exhibits minor differences in the consolidation methods. Deposition of additional Ca-carbonate at the periphery of the disks occurs in both cases (Figure 9d, e for *Pinctada* to be compared with Figure 5h–l for *Pinna*), but this process follows a more ordered way in the former. Contrastingly, further microstructural evolutions of the prisms in the two genera are strikingly distinct. Although the prism single-crystallinity is preserved in *Pinna* (in spite of complexity of the control method), the *Pinctada* prisms are regularly losing this property: they become polycrystalline after some tens of microns of growth as single-crystals (Figure 9f, g) (Dauphin et al., 2019).

Such similarities and differences in microstructural evolution of prisms between two Pteriomorphid prisms have significant implications regarding interpretation of the prismatic microstructures. Formerly, contribution of the periostracum to mineralization process was described by Moynier de Villepoix (1892) in the growing edge of *Anodonta*. He emphasized the role of the periostracum as bearer of the first mineralized elements in shell formation as “round-shaped or irregular units, firstly very distinct then more and more close up to form a polygonal pavement”. Wada (1961), Wilbur (1964), Taylor and Kennedy (1969), Suzuki et al. (2013) have also recognized such circular structures in *Pinctada fucata* as “the result of a spherulitic crystallization process simultaneously producing the prismatic mineral structure and the organic envelopes through a single-phase mechanism”. Following this view, the prisms become polygonal by mutual contact and the growth of the mineral units results in formation of the prism envelopes by “squeezing” the remaining organic components “as impurities to the edges of the growing crystals”.

Contrasting with this interpretation, we have shown that the calcite disks remain independent up to the backward inflexion of the periostracum (Figure 4g; yellow arrows). Formation of a rigid shell is obtained by the additional deposition of calcite by the mantle, materializing the collaborative process between periostracal and outer mantle calcification resulting in very irregular structures (Figure 4j–l). The formation of the true prisms (including envelopes) occurs only in further steps of shell formation.

From an overall viewpoint, the periostracal calcification is a well-established property in some Pelecypod families. For instance, needles with various shapes have been described by Glover and Taylor (2010) in Veneridae. Growing on the outer surface of the periostracum, they built a more or less dense continuous coating on the external surface of the shells. Whilst the role of the calcified structures developed onto the outer side of the periostracum is not obvious, it is not the case in both *Pinna* and *Pinctada*: the circular disks developed on the internal side of the periostracum represent a “flexible shell” predating and structurally contributing to shell formation.

4.2. *Pinna* prisms as individual units: the driving role of organic centres in formation of the first prismatic patterns

Species-specific morphology is an intriguing property of Ca-carbonate biominerals because, associated to the single-crystal behaviour of every microstructural unit, this has long suggested existence of a biological

control over calcium carbonate crystallization. This hypothesis is reinforced by the presence of a complex organic component associated to biominerals with analytical evidences of taxonomy-linked compositions (Dussart, 1983; Samata, 1990; Dauphin, 2003; Marin and Luquet, 2004; Samata et al., 2008; Furuhashi, 2009; Suzuki and Nagasawa, 2013). Many chemical experiments were carried out aiming to reproduce *in vitro* the composite materials whose microstructural and mechanical properties resemble those of naturally produced calcareous biominerals. A first overall interpretation was based on the concept of “shaping crystals with biomolecules” (De Yoreo and Dove, 2004). In this view, specific organic molecules fixed onto the growing crystal faces result in modification of their growth rate, explaining formation of their species-specific morphologies (e.g. Giuffrè et al., 2013). The emerging concept of “mesocrystallization” offers a new space for experimental diversity and frequently opposite interpretations (Cölfen and Antonietti, 2008). Then, Evans (2017) shows that the ion-by-ion model of classical crystallization was not relevant for biocrystallization.

From the study of the calcitic prismatic layers of several species, Checa et al. (2005) suggested that “organic cavities slightly antedate the formation of mineral infilling”, then “prismatic crystals began to form within the organic cavities” and are subject to competitive growth. According to Wolf et al. (2012, p. 13), crystallization of the prism started from organic envelopes: “The phase transformation of the prism to a final crystalline state is triggered heterogeneously by the periprismatic sheaths and proceeds thenceforth in a centripetal manner”. The role of the inter-prismatic membranes in calcitic prisms is still emphasized (Checa et al., 2016). In contrast to these externally driven crystallization models, Bayerlein et al. (2014) calculated that based on morphological variations of the prisms transverse sections during prisms elongation, “the classical theories of normal grain growth completely describe the mesostructure of the prismatic layer of *P. nobilis*”.

Remarks must be made that these distinct interpretations are based only on prisms examined from mature parts of the shell: none of them mention the sequential growth mode of the prisms. As a result, they do not take into account the central nodules produced when outer-mantle mineralization begins (cf. 3.2), every prism comprising a central nodule whose structuring influence is assessed by the Voronoi tessellation. Going back to the Carpenter's observations (reported in Figure 2c) position of the polygon centres with respect to the organic envelopes were clearly drawn, assessing their major role in prism early stages. Suggesting how confident we can be in the Carpenter's observations is also exemplified by the next and probably the most significant step regarding the specificity of the growth of the *Pinna* prism: their linked to the overall growth direction of the whole shell.

4.3. Stepping growth of the shell drives crystallization of the prisms: origin of the prism longitudinal substructures

In the usual simple-prism model, length of the prisms (= thickness of the shell) increases by repeated synchronic deposition of polygonal calcite layers onto prism inner surfaces (Figure 10a). No mention is made of any substructure except in the 1856 Carpenter's description (cf. reported Figure 2d).

The three-dimensional scheme of Figure 10d is obtained by merging data from Figure 8 (dealing with spatial correlation between the oblique growth units visible on the side faces of a given prism) and the stepping growth traces visible on its transverse section (Figure 7). Looking at these oblique structures from a biomineralization point of view, the stepping direction of the shell as a whole is transcribed into prism growth, as shown by the traces of these growth steps, variable in both number and orientation on each of their faces of a given prism.

This leads to conclude that every individual prism is a three-dimensionally oriented structure, strongly contrasting with common views based on non-biologically driven process. This synchronic deposition of mineral material as schematized in Figure 10d draws attention to a major question regarding crystallization of the prisms. The blue and

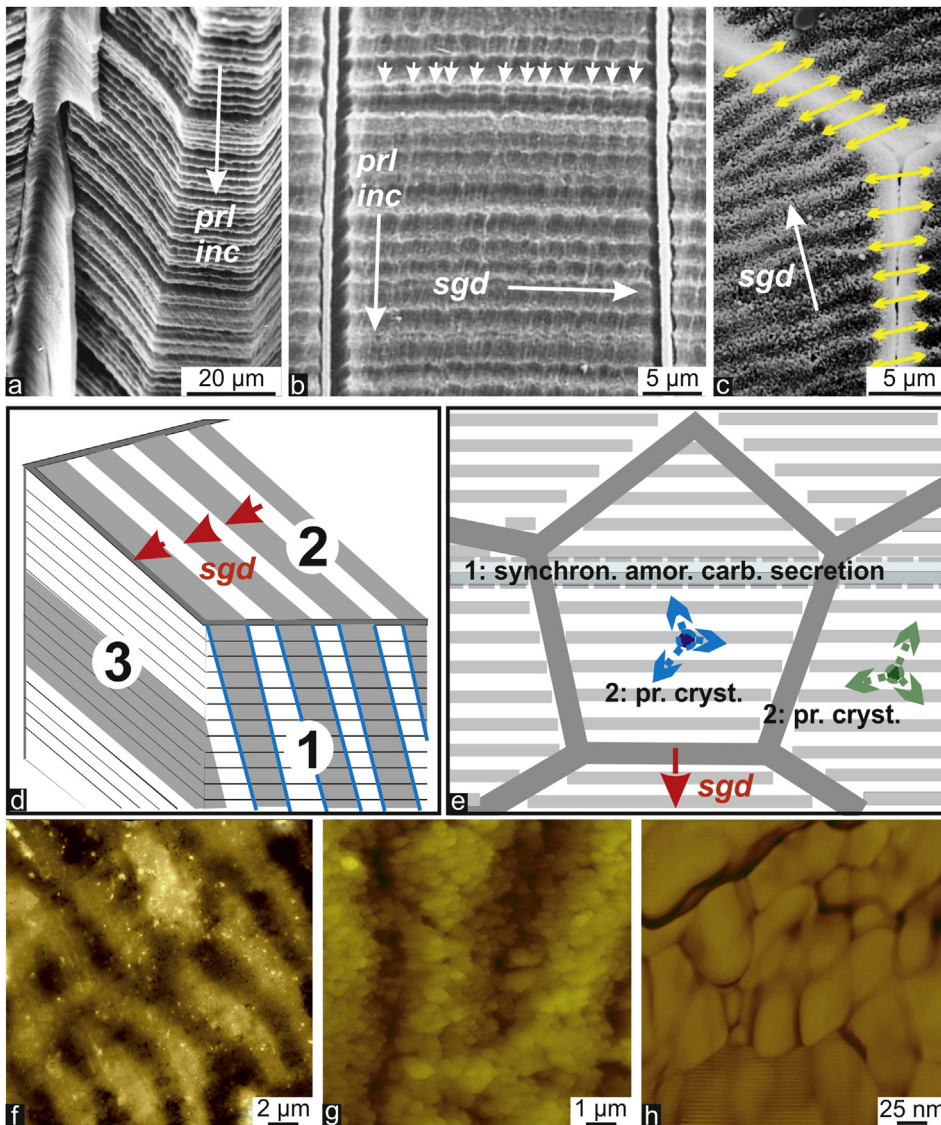


Figure 10. Coordination between thickness increase and lateral extension in the *Pinna* prisms: three-dimensional reconstruction and origin of the internal substructures. a: Components of the “simple prism” scheme: superposed calcite layers wrapped into organic envelope (*prl inc*: prism length increase). b: Longitudinal section showing the ridge and groove system additional to the repeated deposition of the calcite layers (white arrows) *sgd*: shell growth direction. Fixation, etching: glutaraldehyde 12% (100 ml) acetic acid 1% (1 ml) Alcian blue 0.05% (1 ml) 6 min, room temperature. c: Synchronism of the shell growth steps between adjacent prisms: the most spectacular evidence the synchronic elongation of the shell. d: Reconstruction of the coordination between lateral (1) and transverse (2) substructures of the prisms: obliquity of prism substructures is linked to the stepping growth mode of the shell. e: To conciliate crystallographic individuality of each prism and the common deposition of the stepping growth material, hypothesis must be made that the synchronically deposited material (e-1) is amorphous and crystallize according to crystallographic orientation of each of the underlying prisms (e-2). f: Inner surface of an unetched prism showing the ridge and groove structure, AFM height image. g: Detail of the ridge and groove structure in another prism; unetched sample (height image). h: Nanogranules within the prisms, AFM phase image.

green three-arrow diagrams of Figure 10e are reminders of the single-crystal behaviour of every prism (see also Figure 1h): how is it possible to reconcile a common longitudinal stepping growth of the prisms with their long recognized individual crystallographic individuality?

Explanation can be found in Figure 6 dealing with the origin of prismatic individuality and the key role of the centres of calcification. Figure 6a, b has shown that individual crystallographic orientation of every prism is defined in this very early stage, just at the starting point of prisms formation. At this stage (Figure 6k) every young prism has already a specific crystallographic orientation.

To conciliate the common deposition of the calcareous growth units of the shell on its growing edge (Figure 10e), and the long recognized continuity of the specific crystallographic orientation for every prism (e.g., Figure 3f), the hypothesis can reasonably be made that the Ca-carbonate material of the shell growth unit is initially amorphous calcium carbonate. Deposition of this amorphous material at the surface of the adjacent but distinctly crystallized young prisms leads the amorphous material to crystallize according to the crystallographic orientation of each of the underlying prisms acting as distinct substrates. A similar process occurs when the separated disks brought by the periostracum to the growing edge of the growth lamellae (Figure 5c) are cemented by Ca-carbonate deposition that crystallizes according to specific crystallographic orientation of every disk.

Worth to remind that in any step of prism formation, “crystallization” is by no mean an ion-by-ion crystallization process but a still unexplained mechanism leading to formation of the nanogranular organo-mineral composite: see Figures 3e and 10f–h. This explains why no cleavage plans exist within the *Pinna* prisms. Additionally, in *Pinna*, *Pinctada* or any other Invertebrate calcareous skeletons, no evidence has been found for small idiomorph calcite crystals assembled by their lateral faces as postulated by the «mesocrystal» model (Cölfen and Antonietti, 2008).

Examination of the series of structural stages involved in formation of the *Pinna* prisms fully justifies the concept of “directional solidification” (Schoeppler et al., 2018). Of particular significance is the substitution of “solidification” to the usual description of biomineralization as “crystallization”. Previous observations suggest that this concept applies to the *Pinna* prisms not only at the individual scale for every prism, but at the global scale for the shell. Note must be made that such an equivalent property was established for the nacreous layer of the *Pinctada fucata* and numerous other pelecypods by Wada (1961) using X-ray diffraction.

But taking into account the complex microstructural sequence discovered between the early and final developmental stages of the *Pinna* prisms, the sometimes postulated self-organization mechanism (e.g. Böhm et al., 2019) can be hypothesized only at the lowest microstructural level: the formation of the elementary nano-grains. Even at this level, explanation of the coordinated spatial arrangement of the grains

resulting in the remarkably good crystallographic consistency suggests the presence of a leading factor acting at the molecular mechanism. At each of the upper microstructural levels, both envelopes and three-dimensional properties of the mineral phasis assess for presence of specific leading organic phases with relevant genome driven secretory activity.

As a result, the concept of *Pinna* prisms as microstructural reference for “simple prism” appears quite inappropriate. No equivalent growth process has been described among prismatic structures in other Pelecypod families. Taking into account the remarkable preponderance of the prismatic layer in the shells of the Pinnidae family, hypothesis can be suggested that this distinctive property could be linked to a specific growth mode of the prisms. In such case, it should be a singular paradox that the prisms of the *Pinna*, whose morphological simplicity and single-crystal optical behaviour contribute to the widely shared “nacro-prismatic” model for the Pelecypods, appear more an exception than a valid representative of the simple prisms (if any). Therefore, tribute must be paid to these 19th century investigators whose the neglected optical observations paved the way to recent re-examinations.

5. Conclusions

- The outer layer of the *Pinna* shell results of a sequential mineralization process, the first step of which consisting in cementation of the periostracal calcified units by a specific deposition of Ca-carbonate by the mantle epithelium.
- First step in the prismatic microstructural sequence consists in establishing the polygonal organic framework characterized by Voronoi tessellation around punctual organic nodules. Early specific calcification of the prisms with radiating patterns is followed by a short series of synchronically produced calcified layers, with distinct crystallographic orientation for every prism.
- In the following step of the prism developmental process, a distinct mode of calcification is observed. A series of linear depositions occurs synchronically between all the adjacent prisms of the growing area. As crystallographic orientation of this newly deposited material is controlled by the underlying prisms, the previously created prismatic framework is extended. But observation of the resulting substructures in the prisms reveals their individual link to growth direction of the shell. Concomitant formation of the transversal and longitudinal substructures simultaneously ensures the increase of the prism length and shell elongation.
- As *Pinna nobilis* is a critically endangered status (IUCN red list), a better understanding of its shell mineralization process may help to test the health status of individuals.

Declarations

Author contribution statement

Jean-Pierre Cuif: Conceived and designed the experiments; Analyzed and interpreted the data; Wrote the paper.

Oulfa Belhadj, Sergio Trigos-Santos, Patricia Prado: Contributed reagents, materials, analysis tools or data.

Stephan Borensztajn, Marc Gèze: Performed the experiments.

Yannicke Dauphin: Analyzed and interpreted the data; Wrote the paper.

Funding statement

This research did not receive any specific grant from funding agencies in the public, commercial, or not-for-profit sectors.

Competing interest statement

The authors declare no conflict of interest.

Additional information

No additional information is available for this paper.

Acknowledgements

Authors are grateful to Pr. N. Vicente (Université Paul Cézanne and Institut Océanographique Paul Ricard, Les Embiez, France) who made this investigation possible by allowing sampling on actively mineralizing specimens; digital microscope images were acquired by Dr D. De Franceschi (CR2P, Museum National d'Histoire Naturelle, Paris), using a Hirox RH2000 (e-RECOLNAT-ANR-11-INBS-0004 and DIM Ile de France Heritage and ancient materials programs).

References

- Addadi, L., Politi, Y., Nudelman, F., Weiner, S., 2008. Biomineralization design strategies and mechanisms of mineral formation: operating at the edge of instability. In: Novoa, J.J., Braga, D., Addadi, L. (Eds.), *Engineering of Crystalline Materials Properties*. NATO Science for Peace and Security, Series B: Physics and Biophysics. Springer, pp. 1–15.
- Bayerlein, B., Zaslansky, P., Dauphin, Y., Rack, A., Fratzl, P., Zlotnikov, I., 2014. Self-similar mesostructure evolution of the growing mollusc shell reminiscent of thermodynamically driven grain growth. *Nat. Mater.* 12, 1102–1107.
- Böhm, C.F., Harris, J., Schodder, P.I., Wolf, S., 2019. Bioinspired materials: from living systems to new concepts in materials chemistry. *Materials* 12, 2117.
- Bowerbank, J.S., 1844. On the structure of the shells of Molluscan and conchiferous animals. *Trans. Microsc. Soc. Lond.* 1, 123–152.
- Carpenter, W.B., 1844. On the microscopic structure of shells. Part I. *Br. Assoc. Adv. Sci. Rep.* 14, 1–24.
- Carpenter, W.B., 1856. *The Microscope and its Revelations*. John Churchill, London, p. 778.
- Checa, A.G., Rodríguez-Navarro, A.B., Esteban-Delgado, F.J., 2005. The nature and formation of calcitic columnar prismatic shell layers in pteriomorphian bivalves. *Biomaterials* 26, 6404–6414.
- Checa, A.G., Macías-Sánchez, E., Harper, E.M., Cartwright, J.H.E., 2016. Organic membranes determine the pattern of the columnar prismatic layer of mollusc shells. *Proc. R. Soc. B* 283, 20160032.
- Cölfen, H., Antonietti, M., 2008. *Mesocrystals and Nonclassical Crystallization*. John Wiley and Sons, Chichester, UK, p. 288.
- Cuif, J.P., Dauphin, Y., 2018. The Marsh's membrane: a key-role for a forgotten structure. In: Endo, K., Kogure, T., Nagasawa, H. (Eds.), *Biomineralization, from Molecular and Nano-Structural Analyses to Environmental Science*. Springer, pp. 349–357.
- Cuif, J.P., Dauphin, Y., Luquet, G., Medjoubi, K., Somogyi, A., Perez-Huerta, A., 2018. Revisiting the organic template model through the microstructural study of shell development in *Pinctada margaritifera*, the Polynesian pearl oyster. *Minerals* 8, 370.
- Cuif, J.P., Dauphin, Y., Denis, A., Gaspard, D., Keller, J.P., 1980. Continuité et périodicité du réseau organique intra-prismatique dans le test de *Pinna muricata* L. (Lamellibranche). *C. R. Acad. Sc. Paris D* 290, 759–763.
- Cuif, J.P., Denis, A., Gaspard, D., 1981. Recherche d'une méthode d'analyse ultrastructurale des tests carbonates d'invertébrés. *Bull. Soc. Geol. Fr.* 9 (XXIII), 5, 525–534.
- Cuif, J.P., Raguideau, A., 1982. Observations sur l'origine de l'individualité cristallographique des prismes de *Pinna nobilis* L. *C. R. Acad. Sc. Paris* 295 (sér. II), 415–418.
- Dauphin, Y., 2003. Soluble organic matrices of the calcitic prismatic shell layers of two pteriomorphid Bivalves: *Pinna nobilis* and *Pinctada margaritifera*. *J. Biol. Chem.* 278 (17), 15168–15177.
- Dauphin, Y., Brunelle, A., Medjoubi, K., Somogyi, A., Cuif, J.P., 2018. The prismatic layer of *Pinna*: a showcase of methodological problems and preconceived hypotheses. *Minerals* 8, 365.
- Dauphin, Y., Zolotoyabko, E., Berner, A., Lakin, E., Rollion-Bard, C., Cuif, J.P., Fratzl, P., 2019. Breaking the long-standing morphological paradigm: individual prisms in the pearl oyster shell grow perpendicular to the c-axis of calcite. *J. Struct. Biol.* 205, 121–132.
- De Yoreo, J.J., Dove, P.M., 2004. Shaping crystals with biomolecules. *Science* 306, 1031–1032.
- Dussart, G.B.J., 1983. The aminoacid composition of freshwater mollusc shells in relation to phylogeny and environment. *J. Molluscan Stud.* 49 (3), 213–223.
- Evans, J.S., 2017. Polymorphs, proteins, and nucleation theory: a critical analysis. *Minerals* 7, 62.
- Frémy, E., 1855. Recherches chimiques sur les os. *Ann. Chim. Phys. Paris* 3 (43), 47–107.
- Furuhashi, T., 2009. Comparative Biochemical Analysis of Molluscan Shell Organic Matrices. PhD Dissertation. University of Vienna, p. 134.
- Giuffrè, A.J., Hamma, L.M., Hana, N., De Yoreo, J.J., Dove, P., 2013. Polysaccharide chemistry regulates kinetics of calcite nucleation through competition of interfacial energies. *Proc. Nat. Acad. Sci.* 110 (23), 9261–9266.
- Glover, E.A., Taylor, R.J.D., 2010. Needles and Pins: Acicular crystalline periostracal calcification in Venerid bivalves (Bivalvia Veneridae). *J. Molluscan Stud.* 76, 157–179.

- Grégoire, C., 1961. Sur la structure submicroscopique de la conchioline associée aux prismes des coquilles de mollusques. *Inst. Roy. Sc. Nat. Belg. Bull.* 37 (3), 1–34.
- Grégoire, C., 1967. Sur la structure des matrices organiques des coquilles de mollusques. *Biol. Rev.* 42, 653–687.
- Grégoire, C., 1972. Structure of the molluscan shell. In: Florkin, M., Scheer, B.T. (Eds.), *Mollusca*, Col. VII, Chemical Zoology. Academic Press, pp. 45–145.
- Hatchett, C., 1799. XVIII Experiments and observations on shell and bone. *Phil. Trans.* 315–334.
- Haugstad, G., 2012. Atomic Force Microscopy: Understanding Basic Modes and Advanced Applications. John Wiley & Sons, Hoboken, NJ, USA.
- Huxley, T.H., 1880. The Crayfish. An Introduction to the Study of Zoology, 28. Intern. Scient. Series, New York, p. 371.
- Lowenstam, H.A., Weiner, S., 1989. On Biomineralization. Oxford University Press, p. 324.
- Marin, F., Luquet, G., 2004. Molluscan shell proteins. *C.R. Palevol* 3, 469–492.
- Mittal, V., Matsko, N.B., 2012. Analytical Imaging Techniques for Soft Matter Characterization. Springer Science & Business Media, New York, NY, USA.
- Moynier de Villepoix, R., 1892. Recherches sur la formation et l'accroissement de la coquille des mollusques. *J. Anat. Phys. Normales et pathologiques de l'homme et des animaux t. XXVIII* 461–518, 583–674.
- Mutvei, H., 1970. Ultrastructure of the mineral and organic components of molluscan nacreous layers. *Biomineralization* 2, 48–72.
- Nudelman, F., Chen, H.H., Goldberg, H.A., Weiner, S., Addadi, L., 2007. Lessons from biomineralization: comparing the growth strategies of mollusc shell prismatic and nacreous layers in *Atrina rigida*. *Faraday Discuss.*
- Réaumur, R.A.F., 1709. De la formation et de l'accroissement des coquilles des animaux tant terrestres qu'aquatiques, soit de mer soit de rivière. *Histoire de l'Académie Royale des Sciences* 364–400.
- Samata, T., 1990. Ca-binding glycoproteins in molluscan shells with different types of ultrastructure. *Veliger* 33 (2), 190–201.
- Samata, T., Ikeda, D., Kajikawa, A., Sato, H., Nogawa, C., Yamada, D., Yamakasi, R., Akiyama, T., 2008. A novel phosphorylated glycoprotein in the shell matrix of the oyster *Crassostrea nippona*. *FEBS J.*
- Schleiden, M., 1838. Beitrage zur Phytogenesis. *Archiv für Anatomie, Physiologie und wissenschaftliche Medicin Jahrgang*, pp. 137–176.
- Schoeppler, V., Gránásy, L., Reich, E., Poulsen, N., de Kloe, R., Cook, P., Rack, A., Pusztai, T., Zlotnikov, I., 2018. Biomineralization as a paradigm of directional solidification: a physical model for molluscan shell ultrastructural morphogenesis. *Adv. Mater.*
- Schwann, T., 1839. Mikroskopische Untersuchungen über die Uebereinstimmung in der Struktur und dem Wachsthum der Thiere und Pflanzen, p. 268. Berlin, Sander.
- Suzuki, M., Nagasawa, H., 2013. Mollusk shell structures and their formation mechanism. *Can. J. Zool.* 91, 349–399.
- Suzuki, M., Nakayama, S., Nagasawa, H., Kogure, T., 2013. Initial formation of calcite crystals in the thin prismatic layer with the periostracum of *Pinctada fucata*. *Micron* 45, 136–139.
- Taylor, J.D., Kennedy, W.J., 1969. The influence of the periostracum on the shell structure of bivalve Molluscs. *Calcif. Tissue Res.* 3, 274–283.
- Towe, K.M., 1967. Echinoderm calcite: single crystal or polycrystalline aggregate. *Science* 157 (3792), 1048–1050.
- Wada, K., 1961. Crystal growth of molluscan shells. *Bull. Natl. Pearl Res. Lab.* 36, 703–828.
- Weiner, S.W., 1979. Aspartic acid-rich proteins: major components of the soluble organic matrix of mollusk shells. *Calcif. Tissue Int.* 29, 167–193.
- Wilbur, K.M., 1964. Shell formation and regeneration. In: Wilbur, K.M., Owen, G. (Eds.), *Physiology of Mollusca*, ol. 1. Academic Press, pp. 243–282.
- Wolf, S.E., Lieberwirth, I., Natalio, F., Bardeau, J.F., Delorme, N., Emmerling, F., Barrea, R., Kappl, M., Marin, F., 2012. Merging models of biomineralisation with concepts of nonclassical crystallisation: is a liquid amorphous precursor involved in the formation of the prismatic layer of the Mediterranean Fan Mussel *Pinna nobilis*? *Faraday Discuss. Cryst. - Biol. Perspect.* 159, 443–448.